# A NEW PRINTED QUASI-LANDSTORFER ANTENNA

A Thesis
Submitted to the Graduate Faculty
of the
North Dakota State University
of Agriculture and Applied Science

By

Masud Al Aziz

In Partial Fulfillment of the Requirements
for the Degree of
MASTER OF SCIENCE

Major Department:
Electrical and Computer Engineering

May 2011

Fargo, North Dakota

# North Dakota State University
Graduate School

**Title**

A NEW PRINTED QUASI-LANDSTORFER ANTENNA

**By**

Masud Al Aziz

The Supervisory Committee certifies that this ***disquisition*** complies with North Dakota State University's regulations and meets the accepted standards for the degree of

**MASTER OF SCIENCE**

# ABSTRACT

Al Aziz, Masud, M.S., Department of Electrical and Computer Engineering, College of Engineering and Architecture, North Dakota State University, May 2011. A New Printed Quasi-Landstorfer Antenna. Major Professor: Dr. Benjamin Davis Braaten.

In this thesis, a new type of printed quasi-Landstorfer antenna is presented. The proposed antenna utilizes parasitic radiators to realize a higher gain. The antenna is measured to have a resonant frequency of 2.45 GHz with a return loss of -43 dB. The gain of the antenna is measured to be 7.2 dBi and can be increased to 8 dBi with the design of a partial folded slot. The gain increment is achieved without increasing the overall dimension of the antenna. Both the measured and the simulated radiation patterns indicate that the antenna has a symmetric radiation pattern in the end-fire direction. Moment Method based software has been used to simulate this quasi-Landstorfer antenna and the simulated results are shown to be in good agreement with the measured results. The new quasi-Landstorfer antenna presented in this work is 44% smaller in size when compared to the previous Landstorfer antennas and provides higher gain than that of the quasi-Yagi antenna. The antenna is well suited for WLAN band applications, such as wireless communications, phased array antennas, and millimeter wave applications.

# ACKNOWLEDGEMENTS

First, I would like to thank my advisor, Dr. Benjamin D. Braaten, for his support,patience, and guidance in completing this research. He always supported me by providing background necessary for this research. Without his guidance, I would have never been able to complete the research.

I would also like to thank my committee members, Dr. David Rogers, Dr. Sudarshan Srinivasan, and Dr. Alan Denton, for their continuous encouragement and support. They have taught me many things and helped me in overcoming any difficulties I had along the way of this research.

Finally, I would like to thank Aaron Reinholtz and Dr. Michael Reich at Center for Nanoscale Science and Engineering (CNSE) for supporting this research.

# DEDICATION

To my beloved parents and my beautiful wife.

# TABLE OF CONTENTS

# LIST OF FIGURES

# CHAPTER 1. INTRODUCTION

Wireless communication systems are used to transfer information over both short distances and long distances. Short distance wireless communication includes remote control for TV, remote starters for cars, and remote control for air-conditioner units. Long distance wireless communication includes satellite communication, radar communication, and radio communication over hundreds of meters. Today, wireless systems have also been applied to various fields, such as telecommunications, the automobile industry, bill payments, and entertainment. These wireless communication devices need antennas to communicate with each other. Recently, there have been a lot of developments in the wireless communication system which demand more devices to be integrated in a single compact module. Printed antennas are drawing a lot of attention due to their small size, ease of fabrication, and light weight. These printed antennas are employed in the Ultra-High Frequency (UHF) band and above, which leads to small antenna size. Moreover, printed antennas are easy to fabricate on a single dielectric substrate using a lithographic technique. The impedance matching and the phase adjustment of the antenna are done with a microstrip feed structure that can also be printed on the same substrate using the lithographic technique.

A recently developed printed antenna was the planar Yagi-Uda antenna that consists of one driver, one reflector, and one or more director elements [1]. The driver element is excited directly by the feed transmission line. However, the currents in the director and the reflector elements are induced by mutual coupling. Another development based on the planar Yagi-Uda antenna was the quasi-Yagi antenna which uses a truncated ground plane as the reflector and thus eliminates the reflector [2]-[3]. The quasi-Yagi antenna reduces the overall dimension of the printed Yagi-Uda antenna. However, the antenna suffers from a lower gain than that of the Yagi-Uda antenna. A printed Landstorfer design was proposed in [4]-[5], where sweeping

elements were used instead of dipoles as the antenna elements and this resulted to higher gain. However, by the introduction of the sweeping elements, the overall size of the Landstorfer antenna was larger than the printed quasi-Yagi antenna.

In this thesis, we present a new printed quasi-Landstorfer antenna for the 2-4 GHz (S-band) wireless communication applications. The antenna comprises of two sweeping elements with one of the elements being the driver and the other element being the director. In this design, a truncated ground plane is used as the reflector. The antenna has been analyzed both theoretically and practically. Different parameters, such as return loss ($S_{11}$), far-field radiation patterns, and the gain of the antenna have been simulated and measured. The design criteria of the antenna has been described by four parameters, such as *the length of the driver, the distance between the driver and the director, the length of the director, and the distance between the driver and the ground plane.* The impact of each of the parameters on the antenna performance has been examined to find the optimum values. A prototype of the antenna has also been printed and the measurements were taken in an anechoic chamber using an 8.5 GHz Agilent 8057 ENA series network analyzer. The measured results are shown to be in good agreement with the simulated results.

The simulated and the measured results indicate that the proposed quasi-Landstorfer antenna provides a high gain of 7 dBi over a 10 dB bandwidth. The gain of the antenna can be further augmented by introducing a partial folded slot in the design. The antenna has a symmetric radiation pattern in the end-fire direction and is measured to resonate at 2.45 GHz with a return loss of -43 dB.

The rest of the thesis is organized as follows. Chapter 2 presents a brief literature review of the Yagi-Uda antenna, the quasi-Yagi antenna, and the Landstorfer antenna. A review on antenna concepts for the design of the quasi-Landstorfer antenna is presented in chapter 3. This is then followed by presenting the layout of the quasi-

Landstorfer antenna, simulated and measured results, and design guidelines. In chapter 4, a gain enhancement design for the proposed quasi-Landstorfer antenna is presented. Simulated S-parameters, far-field radiation patterns, and the gain of the antenna are also presented at the end of this chapter. Chapter 5 concludes the thesis.

# CHAPTER 2. PREVIOUS WORK

In this chapter, a brief literature review on the Yagi-Uda antenna, the quasi-Yagi antenna, and the Landstorfer antenna is presented. Moreover, the layout of each of the aforementioned antennas is also presented. Simulated S-parameters, far-field radiation patterns, and the gain of the antennas are also discussed.

## 2.1. The Yagi-Uda antenna

### 2.1.1. Wire Yagi-Uda antenna

The Yagi-Uda antenna shown in Fig. 1 consists of a number of dipole elements. One of the dipoles is fed directly by the transmission line. The other dipole elements are excited by mutual coupling and thus act as parasitic radiators.

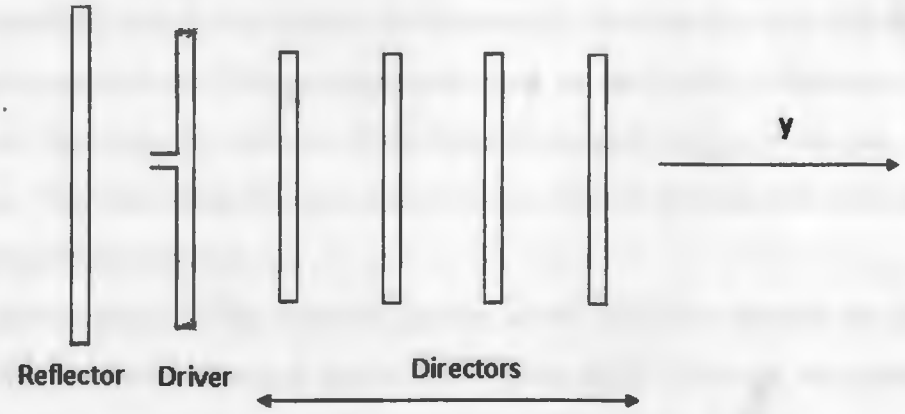


Figure 1. A typical Yagi-Uda antenna configuration.

The element that is fed directly by the transmission line is called the driver. The antenna is designed to have an end-fire radiation pattern by placing the parasitic

elements at the back and in front of the driver element. The elements that are placed in front of the driver are called the directors. Moreover, the elements that are placed at the rear of the driver are called the reflectors. The length of the driver is chosen to be $\frac{\lambda_o}{2}$, where $\lambda_o$ is the free-space wavelength at the resonant frequency. The length of the reflector elements are chosen to be slightly larger than that of the driver element. However, the lengths of the director elements are chosen to be slightly shorter than that of the driver element. Therefore, the impedance of the reflector element is inductive and the induced emf leads the current on the reflector. However, the impedance of the director element is capacitive and the phase of the current leads the phase of the induced emf. Therefore, the Yagi-Uda antenna structure supports a traveling wave propagation along the y-axis of the antenna and the antenna has an end-fire radiation pattern. Moreover, the phase of the current in the parasitic elements also depends on the spacing between the elements.

Among the reflector elements, the nearest reflector element to the driver plays the most significant role on the antenna performance [6]. Besides, the other reflector elements are measured not to have a significant effect on the overall performance of the antenna. However, the addition of the director elements increases the gain of the antenna. Therefore, Yagi-Uda antennas with one reflector element and multiple director elements are common.

The characteristics of the radiation pattern of the Yagi-Uda antenna are expressed by five parameters: *forward and backward gains, input impedance, bandwidth, front-to-back ratio, and magnitude of the minor lobes.* The length of the parasitic radiators and the relative spacing between them determine the antenna characteristics. Antenna impedance is the ratio of voltage to current at the antenna terminal. The front-to-back ratio is the ratio of the gain of the antenna in the maximum direction to the gain of the antenna in the opposite direction. The performance of the Yagi-

Uda antenna is based on *the reflector-feeder arrangement, the feeder, and the rows of directors*. It has been found numerically and experimentally that the length of the reflector and the relative spacing have a negligible effect on the forward gain but have a significant effect on the backward gain and the input impedance [7]. Moreover, the length of the feed and the radius of the feedline have more impact on the backward gain and the input impedance than on the forward gain. However, the length and the spacing of the directors have a significant effect on the forward gain, the backward gain, and the input impedance. Therefore, the size and the spacing of the director elements are considered to be the most critical elements for the design of the Yagi-Uda antenna.

### 2.1.2. The printed Yagi-Uda antenna

A printed Yagi-Uda is shown in Fig. 2. The Yagi antenna is designed on a Rogers 4003 substrate with $\epsilon_r = 3.38$ and thickness of 0.508 mm. The outside dimensions of the antenna are 89 mm $\times$ 78 mm $\times$ 0.508 mm.

The dimensions of the antenna in Fig. 2 are (unit: mm): $W_1 = W_3 = 21, W_2 = 16, W_4 = 28.35, W_5 = 24.3, S_1 = S_2 = 1.3, W_6 = 42, L_1 = 10, L_2 = 28, L_3 = 14, L_4 = 17, L_{ref} = 3, L_{dri} = 2$, and $L_{dir} = 2$. The Yagi-Uda antenna consists of one driver, one reflector, two director elements, and a microstrip balun. The balun acts as an unbalanced to balanced transformer from the co-axial feed line to the driven element. The length of the driver element is $\frac{\lambda_0}{2}$, where $\lambda_0$ is the free-space wavelength at the resonant frequency. The length of each arm of the balun is $\frac{\lambda_0}{4}$ from the ground plane. Moreover, one of the arms of the balun is connected to the ground plane at the bottom layer through a via. Because of this, the two arms of the balun are $180^0$ out of phase with respect to each other. Furthermore, the two arms of the balun excite the two arms of the driven element. Therefore, the two arms of the driver element are $180^0$ out of phase with respect to each other. The $S_{11}$ parameters and the gain of the

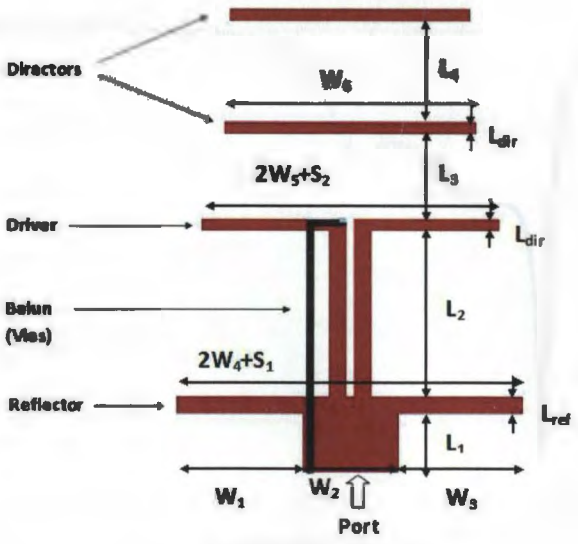


Figure 2. A printed Yagi-Uda antenna. [5]

antenna in Fig. 2 are shown in Figs. 3 and 4, respectively. It is shown in Fig. 3 that the antenna has a simulated (in Momentum [8]) return loss of $-23$ dB at 2.45 GHz. The 10 dB bandwidth of the antenna is 300 MHz from 2.2 GHz to 2.5 GHz. The maximum gain of the antenna is 7 dBi in the 10 dB bandwidth region.

### 2.2. The quasi-Yagi antenna

The schematic of a printed quasi-Yagi antenna is shown in Fig. 5. The antenna is designed for a 1.27 mm thick Rogers 6010 substrate ($\epsilon_r = 10.2$) with metallization on two layers. The top layer consists of a microstrip transition, a microstrip to co-planar stripline transition balun, and two dipole elements, such as the driver and the director element. The driver is fed directly by the transmission line and the director is the parasitic radiator.

The dimensions are (unit:mm):$W_1 = W_3 = W_4 = W_5 = W_{dri} = W_{dir} = 0.6, W_2 = 1.2, W_6 = S_5 = S_6 = 0.3, L_1 = 3.3, L_2 = L_5 = 1.5, L_3 = 4.8, L_4 =$

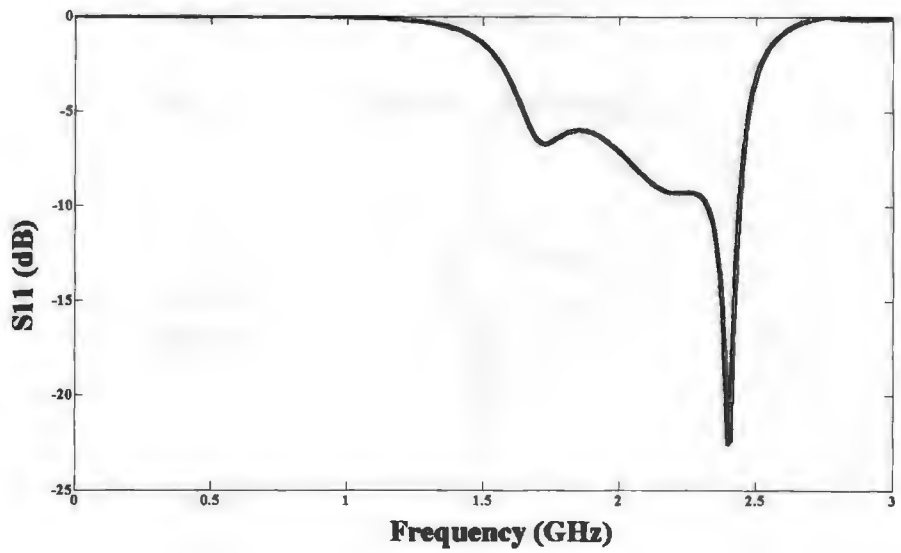


Figure 3. $S_{11}$ of a printed Yagi-Uda antenna.

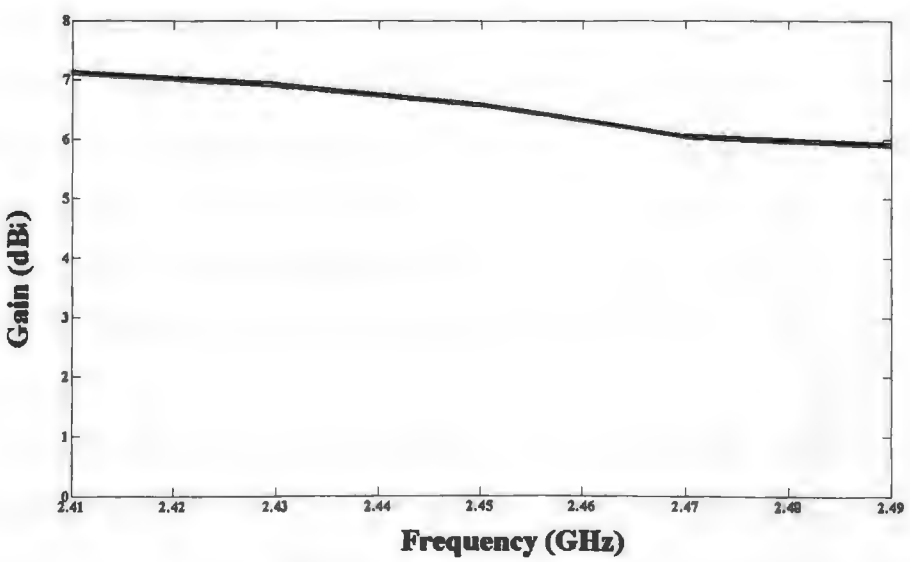


Figure 4. Gain of a printed Yagi-Uda antenna.

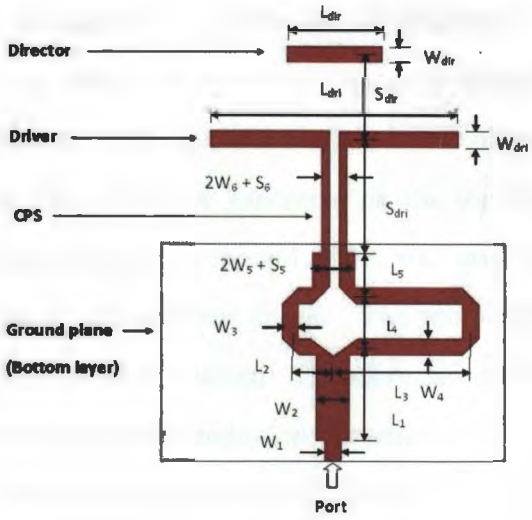


Figure 5. A printed quasi-Yagi antenna.[2]

1.8, $S_{dri} = 3.9, S_{dir} = 3, L_{dri} = 8.7$, and $L_{dir} = 3.3$. The radiation of the quasi-Yagi antenna consists of both the surface wave and the free-space wave. A wave traveling through an ungrounded dielectric slab generates both the $TM_0$ (Transverse Magnetic) and the $TE_0$ (Transverse Electric) modes as the dominant modes of the surface wave. However, a wave traveling through a grounded dielectric slab generates only the $TM_0$ mode as the dominant mode whereas the $TE_0$ mode is at cut off. The reason is that the grounded conductor restricts internal electric fields and continuity across the dielectric/air boundary, therefore, forcing the tangential electric field at the surface to be zero [6].

The driver element in the quasi-Yagi antenna generates the $TE_0$ and the $TM_0$ mode surface waves. The director is coupled to the driver by the $TE_0$ mode surface wave. Moreover, the driver and the director elements are of the same polarization. Therefore, $TE_o$ surface wave from the driver strongly couples the director element. However, the coupling of $TE_o$ surface wave also depends on the spacing between

the elements and the dielectric constant of the substrate. The director acts as an impedance matching element and directs energy propagation towards the endfire direction. In the bottom layer, the $TE_0$ mode is at cut off and thus acts as a reflector to the $TE_0$ surface wave that was generated on the top layer. In the design of the quasi-Yagi antenna, a truncated ground plane was used as the reflector and thus eliminates the need of the reflector dipole. The grounded portion of the antenna produces the endfire radiation pattern. Therefore, no dipole element or metal plate is needed to produce the endfire radiation pattern.

The role of the driver element in the quasi-Yagi antenna is different than the role of the driver element in the Yagi-Uda antenna. The driver in the quasi-Yagi antenna is used to generate surface wave power in a high dielectric constant substrate on which the antenna is printed. The driver produces the $TE_o$ (Transverse Electric) mode surface wave that contributes to the mutual coupling between the driver and the director. The grounded portion of the antenna acts as a reflector for the $TE_o$ mode surface wave and thus produces the endfire radiation pattern. The cutoff frequency for the radiation of the microstrip transmission line is usually higher than the S- or X-band frequencies, as will be described later. Therefore, the $TE_o$ mode surface wave can be used to produce the desired endfire radiation pattern.

The quasi-Yagi antenna in Fig. 5 was simulated using the Advanced Design System (ADS) software from Agilent Technologies [8]. The $S_{11}$ parameters of the antenna are shown in Fig. 6. The antenna has a 10 dB bandwidth from 8 GHz to 12 GHz. The gain of the antenna is shown in Figure 7. The antenna has a gain of 5 dBi over the 10 dB bandwidth.

### 2.3. The Landstorfer antenna

The traditional approach of designing a high gain antenna is to design a Yagi-Uda antenna. It has been shown that the gain of an antenna can be further augmented

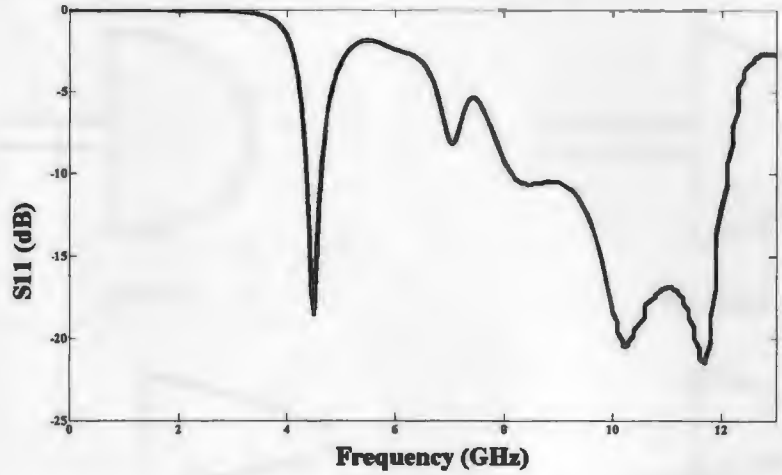


Figure 6. $S_{11}$ of a printed quasi-Yagi antenna.

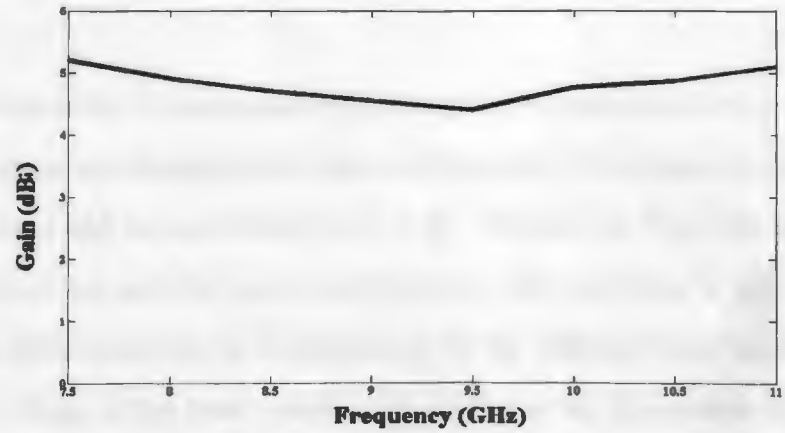


Figure 7. Gain of a printed quasi-Yagi antenna.

by shaping the conductors in a particular manner [4]. For example, Fig. 8 shows the current distribution on a dipole for different lengths.

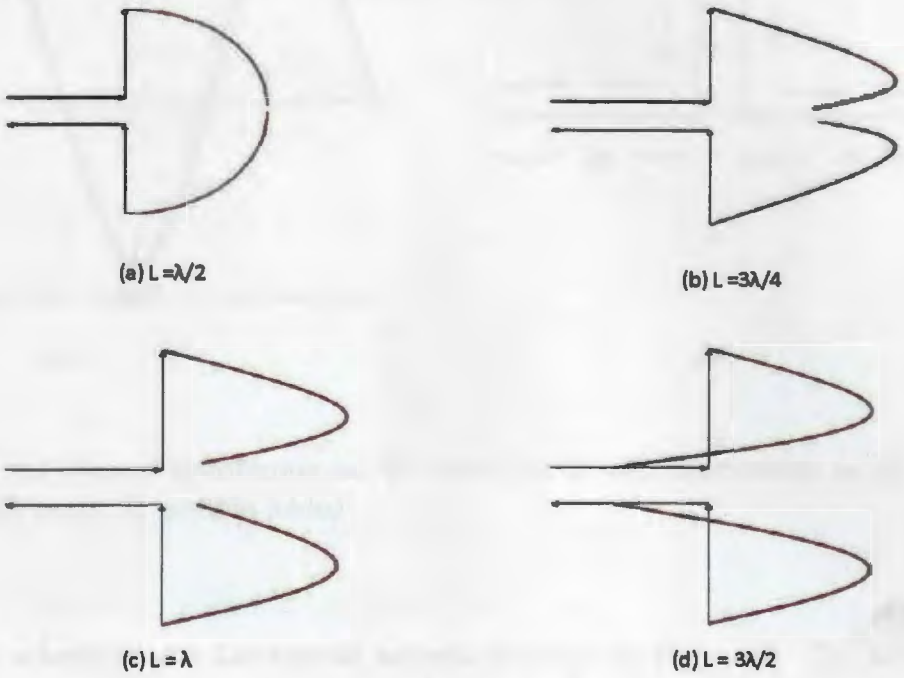


Figure 8. Current distribution on various center-fed dipoles.

The directivity of an antenna with a length, L is maximum for $L = \frac{\lambda_0}{2}$, where $\lambda_0$ is the free-space wavelength at the resonant frequency. The reason is that the phases of the currents add to each other for $L = \frac{\lambda_0}{2}$. However, in Figs. 8b-8d, the phases of the currents are not the same and therefore, the directivity is not a maximum. The phase differences can be compensated for by different path lengths using the appropriate shape of the linear antenna [4]. In Figure 9a, the current distribution on a $\frac{3\lambda_0}{2}$ dipole is shown. The center $\frac{\lambda_0}{2}$ portion of the $\frac{3\lambda_0}{2}$ dipole is then segmented into a $\frac{\lambda_0}{4}$ stub as shown in Fig. 9b. By doing this, the phases of the currents cancel each other on the stub whereas the phases of the current add to each other in the linear portion. Therefore, the antenna behaves as an $1\lambda_0$ in phase dipole antenna.

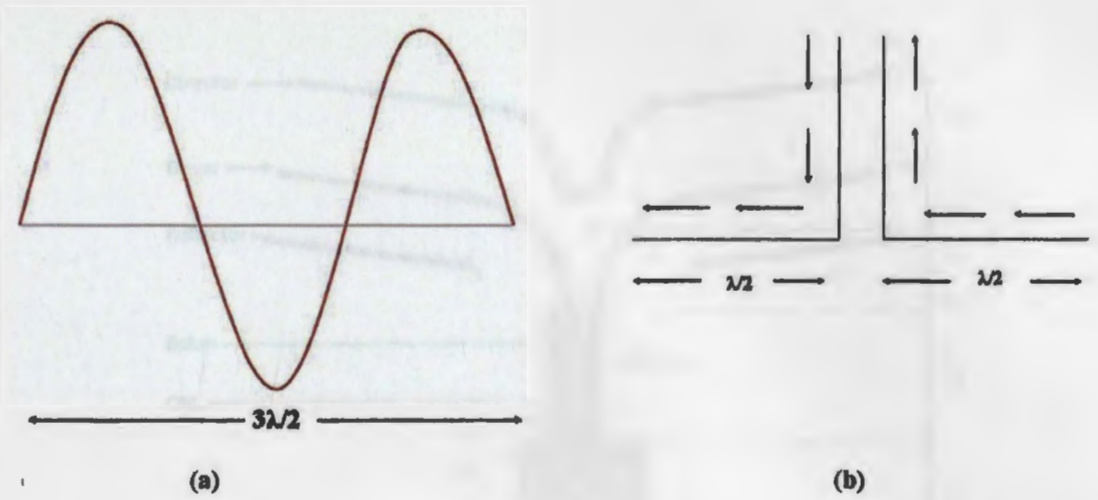


Figure 9. (a) Current distribution on $\frac{3\lambda_0}{2}$ dipole (b) Current distribution on $\frac{3\lambda_0}{2}$ dipole with center $\frac{\lambda_0}{2}$ portion folded

The schematic of a Landstorfer antenna is shown in Figure 10. The antenna is designed on a Rogers 4003 substrate with $\epsilon_r = 3.38$ and a thickness of 0.508 mm. The overall dimension of the antenna is 160 mm $\times$123 mm $\times$0.508 mm.

The dimensions are (unit:mm): $W_1 = 30, W_2 = 1.2, W_3 = 0.4, W_4 = 2, W_5 = 3.5, W_6 = 3.3, W_7 = 72.5, W_8 = W_9 = 4, L_1 = 30, L_2 = 31, L_3 = 7.2, L_4 = 10.5, L_5 = 15.1$, and $L_6 = 22$. The Landstorfer antenna consists of a driver, a director, a reflector, and a microstrip balun. The balun acts as an unbalanced to balanced transformer from the feed co-axial line to the driven element. The length of the driver element is $\frac{\lambda_0}{2}$, where $\lambda_0$ is the free-space wavelength at the resonant frequency. The simulated $S_{11}$ and the gain of the proposed quasi-Landstorfer antenna is shown in Figs. 11 and 12, respectively. The antenna has a simulated return loss of $-19$ dB at 2.45 GHz and a simulated gain of 9 dBi over the 10-dB bandwidth.

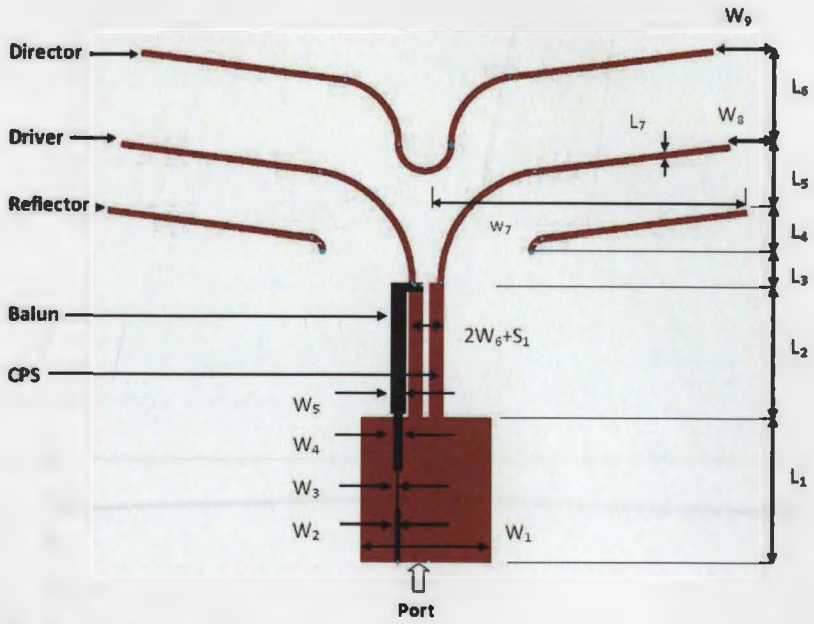


Figure 10. A printed Landstorfer antenna.[5]

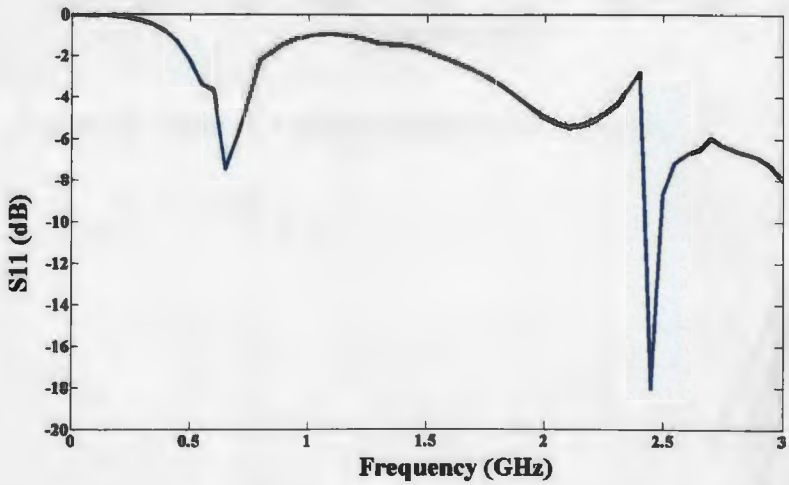


Figure 11. $S_{11}$ of a printed Landstorfer antenna.

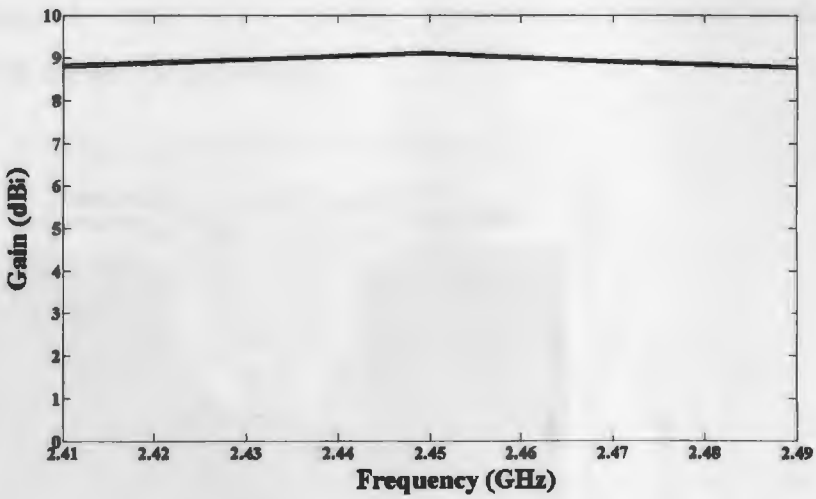


Figure 12. Gain of a printed Landstorfer antenna.

# CHAPTER 3. THE NEW PRINTED QUASI-LANDSTORFER ANTENNA

In this chapter, a new printed quasi-Landstorfer antenna is presented. A drawing of the proposed quasi-Landstorfer antenna is shown in Figure. 13. The dimensions are (unit: mm): $v = 26.3, g = 9.0, q = 1.5, c = 9.5, s = 9.5, r = 20.74, b = 10.69, t = 7.2, n = 1.2, d = 3.66, k = 10.2, m = 2.4, H = 82.0, D = 114.35$, and $W = 132.67$. This chapter starts with the analysis of some antenna concepts. This is then followed by presenting the layout of the antenna. Measured and simulated results are also presented at the end of this chapter.

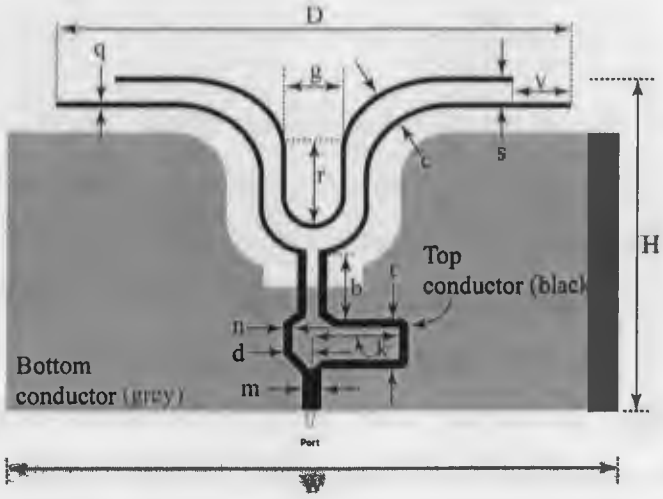


Figure 13. Schematic of quasi-Landstorfer antenna.

## 3.1. Theory

Microstrip antennas radiate from the currents induced on the antenna elements or from the magnetic currents around the periphery of the antenna element. In addition to radiation, surface waves are also excited from the currents induced on the

dielectric slab. Moreover, the surface waves radiate at the edge of the substrate. The surface waves are TE (Transverse Electric) and TM (Transverse Magnetic) waves that propagate in the substrate and outside the microstrip antenna element. The modes are characterized by waves attenuating in the transverse direction (normal to the antenna plane) and having a real wave number in the direction of propagation. The fringing fields from the metal layer to the ground plane excite the lowest order surface wave $TM_0$ that has no cut-off frequency. The generation of higher order TM and TE surface waves depends on the dielectric constant and the thickness of the substrate. The cut-off frequencies for higher order modes are given by the follwing equation [9]:

$$f_c = \frac{nc}{4h\sqrt{\epsilon_r - 1}} \tag{1}$$

where c is the velocity of light in free space, h is the thickness of the substrate, $\epsilon_r$ is the relative permittivity of the substrate, $n = 1, 3, 5..$ for $TE_n$ modes, and $n = 2, 4, 6..$ for $TM_n$ modes. Equation (1) states that the lower order surface wave modes are generated with an increase in thickness and an increase in dielectric constant of the substrate. Surface wave radiation results in low-radiation efficiency, high cross-polarization radiation, and strong mutual coupling [9]. Therefore, surface wave radiation does not contribute to the main beam radiation and thus can be considered as a loss mechanism. The radiation efficiency is defined as:

$$e = \frac{P_{rad}}{P_{rad} + P_{sw}} \tag{2}$$

where $P_{rad}$ is the radiated power in free-space (main beam power) and $P_{sw}$ is the power coupled to the surface wave. $(P_{rad} + P_{sw})$ is the total power delivered to the antenna element. From Equation (2) it is observed that high surface wave power results in low radiation efficiency.

In the quasi-Yagi antenna, the driver element was used to generate the $TE_0$ mode surface wave power on the metal layer to obtain the endfire radiation pattern. On the bottom layer, the $TE_0$ mode was at cut-off and therefore, the ground plane was used as the reflector for the generated $TE_0$ mode on the top layer. The $TE_0$ mode on the top layer was also used to couple the driver and the director elements. However, the $TE_0$ mode surface wave power was generated using a thick substrate with a high dielectric constant. In the proposed quasi-Landstorfer antenna, no surface wave power was generated to contribute to the radiation pattern. The substrate was chosen to have a dielectric constant of 3.38 with a thickness of 0.508 mm. It was shown in [10]-[11] that for $(h < 0.01\lambda_0)$, the surface wave power was negligible. According to Equation (1) it can be shown that the cut-off frequency for the surface wave in the substrate used for this work is 39 GHz. The proposed quasi-Landstorfer antenna is designed to operate at 2.45 GHz. Therefore, the quasi-landstorfer antenna can realize better radiation efficiency than that of the quasi-Yagi antenna.

In the proposed quasi-Landstorfer antenna in Fig. 13, the driver element of the antenna is fed by a microstrip-to-coplanar stripline transmission line. The balun for this antenna serves as a transition for a microstrip line and a Co-Planar Strip-line (CPS). The microstrip lines at the input port as well as the two split arms to the CPS are all assumed to be $50\Omega$. The balun employs a quarter-wavelength long, $34.5 - \Omega$ impedance transformer, followed by a symmetric T junction for signal dividing or combining.

The quarter-wave transformer, as shown in Figure 14, is a section of transmission line, $\frac{\lambda}{4}$ long, used to match the input impedance of the T-junction ($R_L = 25\Omega$) to the $50\Omega$ input impedance of the microstrip line. First, $Z_{in}$ is found by looking into the $\frac{\lambda}{4}$ section by:

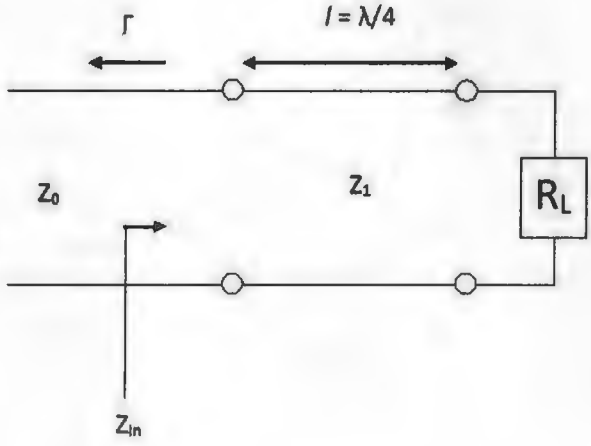


Figure 14. Quarter-wave transformer.

$$Z_{in} = Z_1 \frac{R_L + jZ_1 \tan \beta l}{Z_1 + jR_L \tan \beta l} \tag{3}$$

where $\beta l = (\frac{2\pi}{\lambda}).(\frac{\lambda}{4}) = \frac{\pi}{2}$. Next, the limit $\frac{\beta l}{2} \rightarrow \frac{\pi}{2}$ is used in (3) and both numerator and denominator are divided by $\tan \beta l$ resulting in

$$Z_{in} = \frac{{Z_1}^2}{R_L}. \tag{4}$$

To find $Z_1 = 35.4\Omega$, for $\Gamma = 0$ looking into the $\frac{\lambda}{4}$ section, $Z_0 = Z_{in}$ which yields

$$Z_1 = \sqrt{Z_0 R_L}. \tag{5}$$

The symmetric T-junction line is a simple three-port network used for power dividing or combining in any type of transmission line medium. The T-junction used here is assumed to be lossless, $B = 0$ and is modeled by three transmission lines, $Z_0$, $Z_1$, and $Z_2$ as shown in the Figure 15.

The input admittance can be written as:

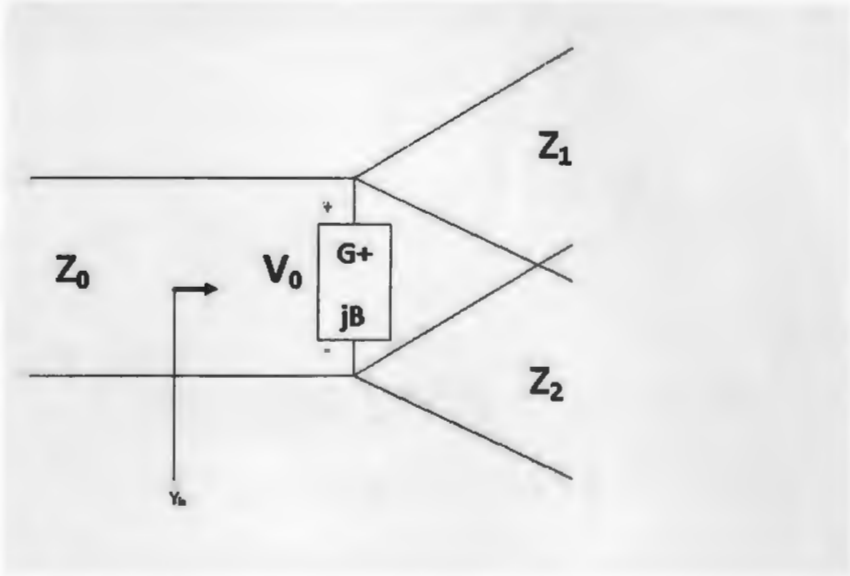


Figure 15. Lossless T-junction line.

$$Y_{in} = \frac{1}{Z_1} + \frac{1}{Z_2} + G + jB \tag{6}$$

$$\frac{1}{Z_1} + \frac{1}{Z_2} = \frac{1}{Z_0} \tag{7}$$

Since equal power split is desired (3 dB) for $Z_1$ and $Z_2$ (50Ω each), the input line must be 25Ω.

The transition is implemented by branching off the single microstrip line into two lines. Then a $180^0$ phase shift is achieved between the two arms by adjusting the lengths with a difference of $\frac{\lambda_g}{4}$, where $\lambda_g$ is the guided wavelength in the microstrip.

### 3.2. Layout

A photograph of the proposed quasi-Landstorfer antenna is shown in Figure. 16.

The overall structure is comprised of a feeding portion, a driven portion, and

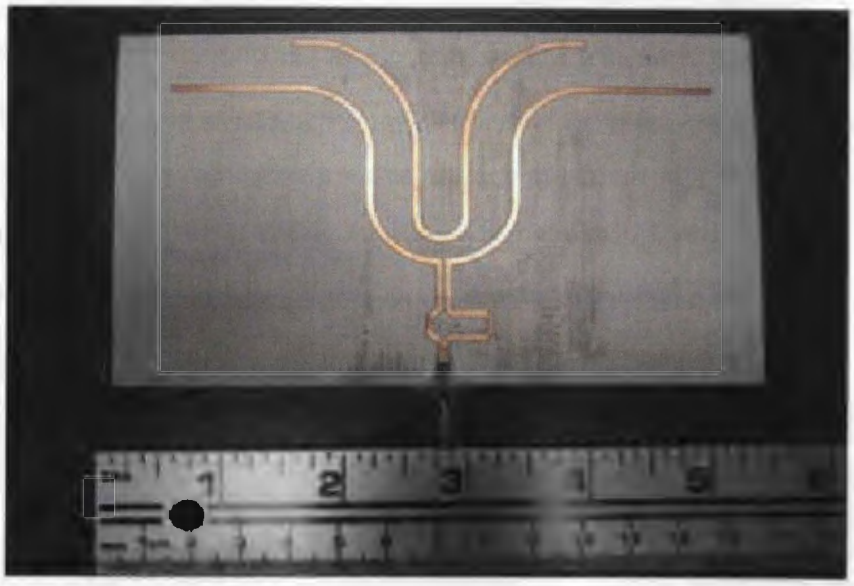

Figure 16. A photograph of the prototype quasi-Landstorfer antenna.

a reflector portion with metallization on two layers. The top layer consists of the feeding part and the driven part. The driven part consists of the swept dipole with a length D (as shown in Figure 13) and the swept director. In the feeding part, two arms of the microstrip line constitute the transition part that transmits energy from the SMA connector to a Co-Planar Stripline (CPS) that drives the swept dipole. The guided wavelength, $\lambda_g$ was calculated with the aid of commercial software package, Applications Computer Aided Design Program (AppCAD) [12].

The director increases the front-to-back ratio. The front-to-back ratio is the ratio of the gain in the maximum direction to that in the opposite direction [6]. Furthermore, the parasitic element is used for matching [14]. The use of additional director elements could further enhance the gain of the antenna.

In the driven portion, sweeping or curved elements are introduced to create a longer electrical path for the current to travel that eventually leads to a higher gain.

The metallization on the bottom layer comprises of a truncated ground plane that is used as a reflector. The ground plane is truncated in parallel to the driven element to reflect most of the electromagnetic waves in the y-direction. Moreover, the truncated ground plane also serves as the ground for the microstrip feed line of the antenna. Metallization on both the top and the bottom layers also ensures the overall structure will be mechanically stable.

The antenna in Fig. 13 was designed to operate in the *S*-band at 2.45 GHz. The antenna was fabricated on a Rogers 4003 substrate ($\epsilon_r = 3.38$) with dimensions 133 mm x 82 mm x 0.5 mm and is shown in Fig. 16. The performance of the quasi-Landstorfer antenna depends on careful optimization of the lengths of the driven element, the distance between the driven element and the reflector, the length of the parasitic element, and the distance between the driven element and the director.

## 3.3. Simulated and measured results

### 3.3.1. S-parameters

The simulated and measured S-parameters of the prototype antenna are shown in Figure 17. It is shown in Figure 17 that the proposed antenna has a simulated return loss of -16 dB at 2.45 GHz. The measurements were taken in an anechoic chamber using an 8.5 GHz Agilent 8057 ENA series network analyzer. The measured results are shown to be in a good agreement with the simulated results. The antenna was measured to have a return loss of -43 dB at 2.44 GHz. The 10 dB bandwidth of the antenna was measured to be 60 MHz. This is also in good agreement with the simulated results.

### 3.3.2. Radiation pattern

The radiation patterns of the antenna were measured in the x-z and y-z planes. The setup of the measurement system is shown in Figs. 18 and 19 for the y-z and x-z

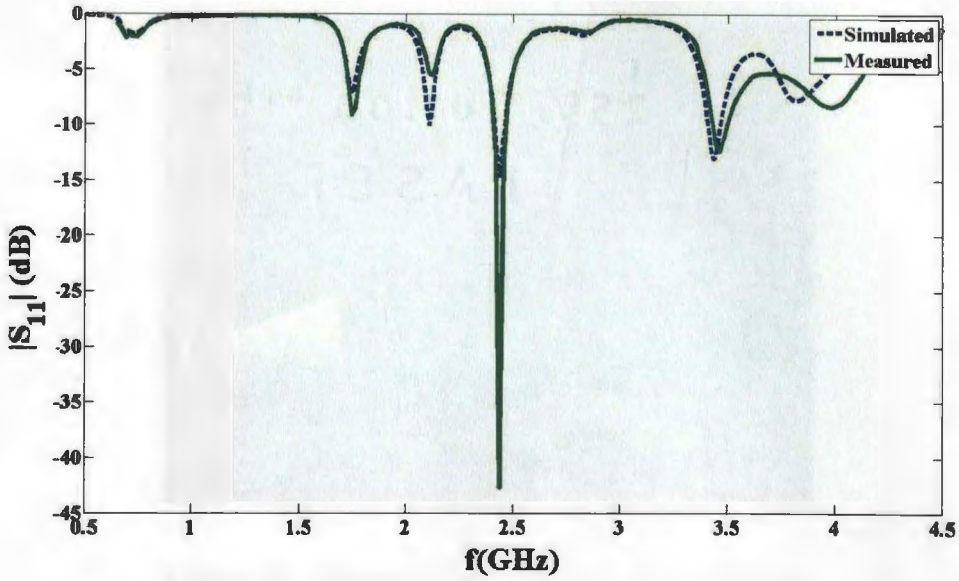


Figure 17. $S_{11}$ of the quasi-Landstorfer antenna.

planes respectively. A horn antenna of the HRN-0118 series from TDK Inc. [18] was used as the transmitting antenna.

The simulated and measured values are shown to agree well in Figs. 20 and 21 for the x-z and y-z planes, respectively. Both the simulated and measured results in Figs. 20 and 21 confirm that the antenna has an end-fire radiation pattern. In the y-z plane, the measurements were conducted twice from $0^o$ to $180^o$ to get the $360^o$ pattern. Therefore, there is an overlapping of the measured data in the y-z plane at $\theta = 90^o$. However, Fig. 20 shows well defined end-fire radiation.

### 3.3.3. Gain

The gain of the antenna was measured through $S_{21}$ values. A TDK Inc. horn antenna (HRN-0118) [18] was used as the transmitting antenna and was connected to port 1 of the network analyzer. A reference bilogical antenna (AK-521F-4 series from A. H. Systems, Inc.) [19] was connected to port 2 of the network analyzer and

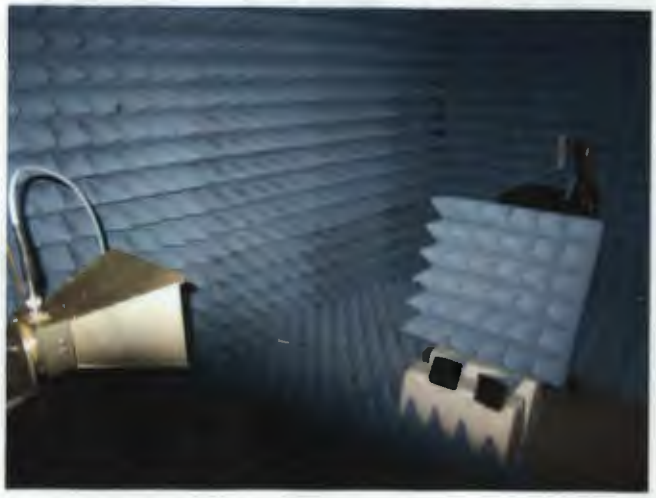

Figure 18. Measuring the radiation pattern in the y-z plane in an anechoic chamber.

Figure 19. Measuring the radiation pattern in the x-z plane in an anechoic chamber.

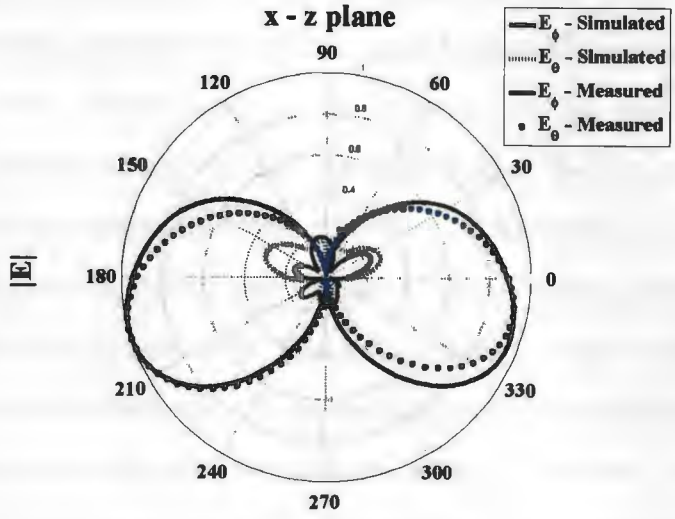


Figure 20. Simulated and measured radiation patterns in the x-z plane at 2.45 GHz.

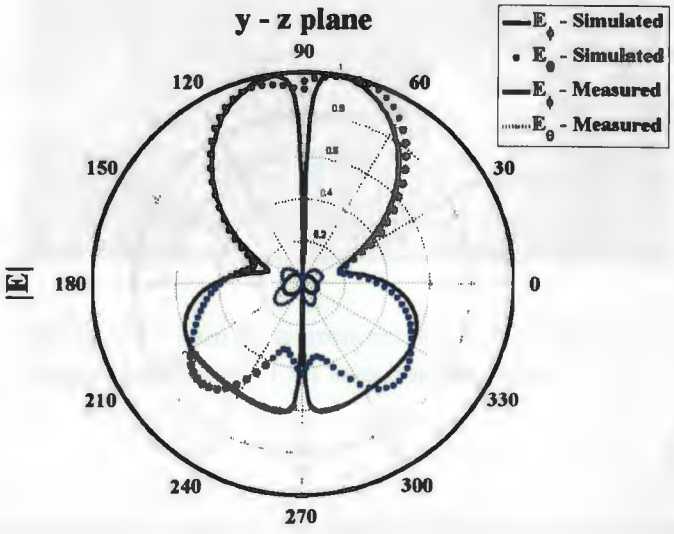


Figure 21. Simulated and measured radiation patterns in the y-z plane at 2.45 GHz.

the $S_{21}$ values were measured. This was considered to be the reference value. Then the bilogical antenna was removed and the quasi-Landstorfer antenna was connected to the port 2 of the network analyzer. At this stage, the $S_{21}$ values were measured and this was considered to be the test case. The gain of the antenna was computed from the difference between these two $S_{21}$ values. If the reference $S_{21}$ values were 2 dBi less than the test $S_{21}$ values, then the gain of the antenna is positive by 2 dBi and vice versa. The photographs of the gain measurement system is shown in Fig. 22. The simulated and the measured gain of the antenna is shown in Figure 23. It should also be noted that the cable loss between the antenna positioner and the biological antenna in Fig. 22 was measured and included in the gain computations.

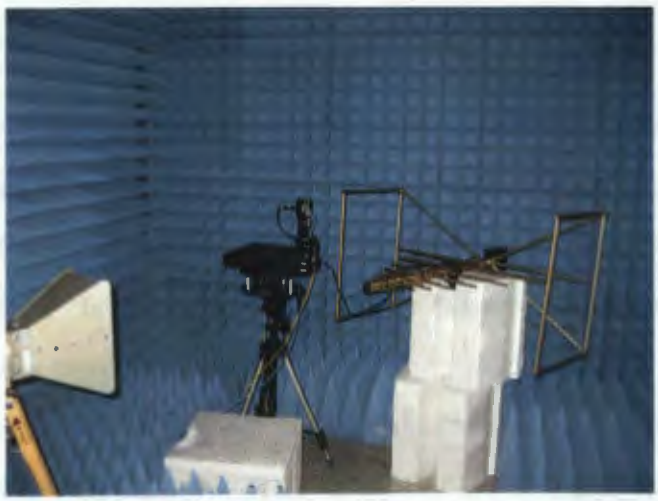

Figure 22. Gain measurement setup with reference bilogical antenna in an anechoic chamber.

The gain of the quasi-Landstorfer antenna depends on the sweeping angles of the elements. The gain also depends on careful optimization of the length of the director element, the driver element, and the reflector element. The spacing between the driver and the director elements as well as spacing between the driver and the

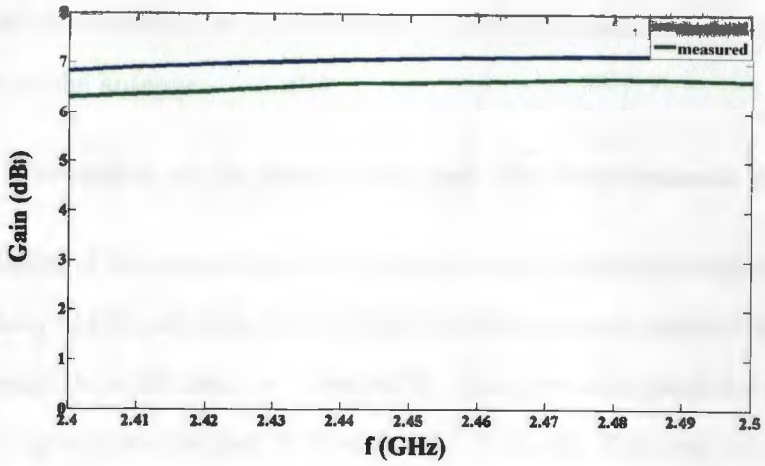


Figure 23. Simulated and measured gain of the quasi-Landstorfer Antenna.

reflector element also affect the gain of the antenna. The maximum gain of the antenna was found to be 7.1 dBi. The simulated and the measured gain over the 10-dB bandwidth of the antenna is shown in Fig. 23. However, it is worth mentioning here that the gain of the antenna can be further enhanced by introducing a partial slot that will be discussed in chapter 4.

The measurements were taken in an anechoic chamber using an 8.5 GHz Agilent 8057 ENA series network analyzer. The far field of the antenna was found from the equation as below [6]:

$$S \geq \frac{2D^2}{\lambda_0} \tag{8}$$

where, $S$ is the minimum distance of the far-field, $D$ is the maximum dimension of the antenna and $\lambda_0$ is the free-space wavelength. For the quasi-Landstorfer antenna to operate in the S-band, the far-field was found to be 0.29m. In the measurement setup, the distance between the transmitting antenna and the quasi-Landstorfer antenna was

fixed at 1.42 m. Therefore, it is evident that all of the measurements were taken in the far-field of the antenna.

### 3.4. Discussion of the simulation and the measurement results

The design of the quasi-Landstorfer antenna was simulated using the Advanced Design System (ADS) software that is based on the moment method [8]. The mesh size was chosen to be 50 cells per wavelength. The generated mesh for a simulation establishes a geometric complexity of a circuit. A design that can be accomodated to a set of rectangular meshes is considered to be less complex. However, the more number of triangular meshes that are needed to cover the design, the more complex the design becomes [17]. The complexity of a design is defined as:

$$Complexity = \frac{numberoftriangles}{numberofrectangles} \tag{9}$$

Therefore, larger mesh size values increase the complexity of the antenna design. However, very low mesh size values tend to cover even geometrically non-linear shapes, such as circles, ellipses, and parabolas with rectangular meshes. Therefore, to provide accurate results, it was experimentally determined that the mesh size for the simulation of this design should be 50 cells per wavelength.

Another important parameter in the simulation process is the selection of the ports. The ports are inserted at the end of the transmission line to excite the antenna. Two types of ports, such as single mode and internal ports can be used in ADS. The internal ports can be inserted anywhere into the design. The internal port assumes a lumped voltage source at the place of insertion and does not calibrate out the effect of the voltage source in the calculation of the S-parameters. However, the single mode port has to be inserted at the end of the transmission line feeding the antenna and it assumes a voltage source at a distance of a half wavelength from the

feeding transmission line. Excitation by the single mode calibrates out the effect of the voltage source in the calculation of S-parameters. Therefore, in the simulation of the quasi-Landstorfer antenna, the single-mode port was used to excite the antenna and the transmission line network feeding the antenna.

In Figs. 17, 20, 21, and 23, it is shown that the simulated and the measured results agree very well. However, some of the differences may be due to the effect of parallel-plate modes. A parallel-plate mode is a special case of surface-wave modes [17]. Parallel-plate modes exist between printed conductor and ground plane. The fundamental parallel-plate mode has no cut-off frequency and is excited by any current source. The higher order modes have a cut-off frequency and the modes decay exponentially below this cut-off frequency. The fundamental mode generates an electric field around the plates and thus establishes a potential difference between the two plates. The generated electric field behaves as a cylindrical wave that propagates along the z-axis to infinity. The reason for propagating to infinity is that ADS assumes the plates to be short-circuited at infinity. Therefore, the electric field generated by the fundamentel parallel-plate mode assumes no reflection in the simulation. However, practically, the two plates are tied together at the edge of the substrate and not at infinity. Therefore, the electric fields of the fundamental parallel plate modes generate reflection of the cylindrical waves from the edge of the substrate. The reflection of the waves from the edges of the substrate might create differences between the simulated and the measured results.

## 3.5. Design guidelines

The design guidelines of the quasi-Landstorfer antenna is based on four different parameters:

- The length of the driver
- The spacing between the driver and the director
- The length of the director
- The spacing between the driver and the ground plane

The effect of each of the aforementioned parameters is discussed below.

### 3.5.1. The length of the driver

The length of the driven element was chosen to be $\frac{3\lambda_o}{2}$. The linear portion of the driver was chosen to be $\lambda_o$ and the sweeping portion was chosen to be $\frac{\lambda_o}{2}$ where the phase of the currents at the two arms cancel each other. Different lengths of the driver element is examined in ADS and is shown in Fig. 24.

It is shown in Figure 24 that the antenna with a driver length of 170 mm has a return loss of -18 dB at 2.45 GHz. The antenna with a driver length of 160 mm has a greater return loss but the resonant frequency goes beyond our desired frequency band. Therefore, the driver length of 170 mm is the optimum value in this case and is also equal to $\frac{3\lambda_o}{2}$.

### 3.5.2. The spacing between the driver and the director

The spacings between the driver and the director element has an impact on the forward gain, backward gain, and the input impedance [7]; this effect is investigated in the next section. Different spacings between the two elements have been examined as shown in Figs. 25 and 26.

It is shown in Figs. 25 that the antenna has an optimum spacing of 9.66 mm with a return loss of -18 dB at 2.45 GHz. The highest gain can also be realized with

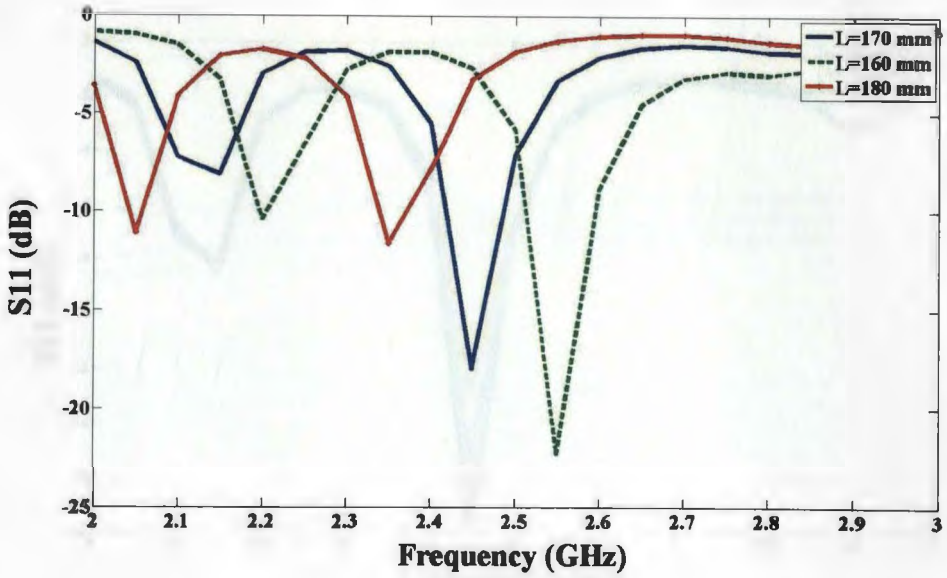


Figure 24. Simulated S-parameters for different driver lengths.

this spacing as shown in Fig. 26. Therefore, the optimum value was chosen to be 9.66 mm.

### 3.5.3. The length of the director

The length of the director also affects the gain and the input impedance of the antenna [15]. Simulated results with different lengths of the director are shown in Figs. 27 and 28.

It is shown in Figure 27 that the director with a length of 150 mm has a better return loss than that of a director with 130 mm. However, it can be seen in Figure 28 that the director with 130 mm has an 1 dBi higher gain than that of the director with 150 mm. Therefore, the optimum value of the director was chosen to be 130 mm.

### 3.5.4. The spacing between the driver and the ground plane

The spacing between the driver and the ground plane affects the input impedance

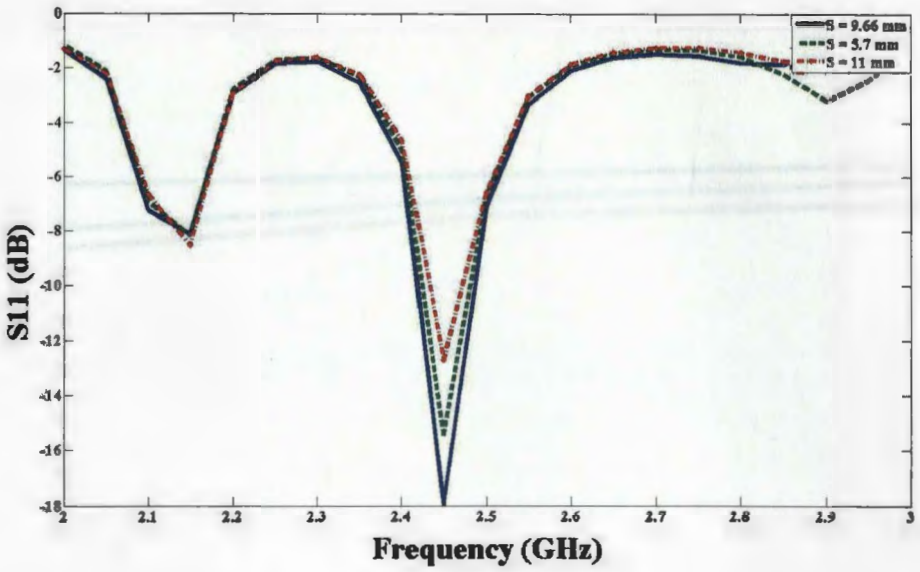


Figure 25. Simulated S-parameters for different driver-director spacings.

of the antenna as shown in Fig. 29. It is shown that the antenna has a maximum return loss of -18 dB with the spacing of 5 mm. Therefore, this is the optimum value.

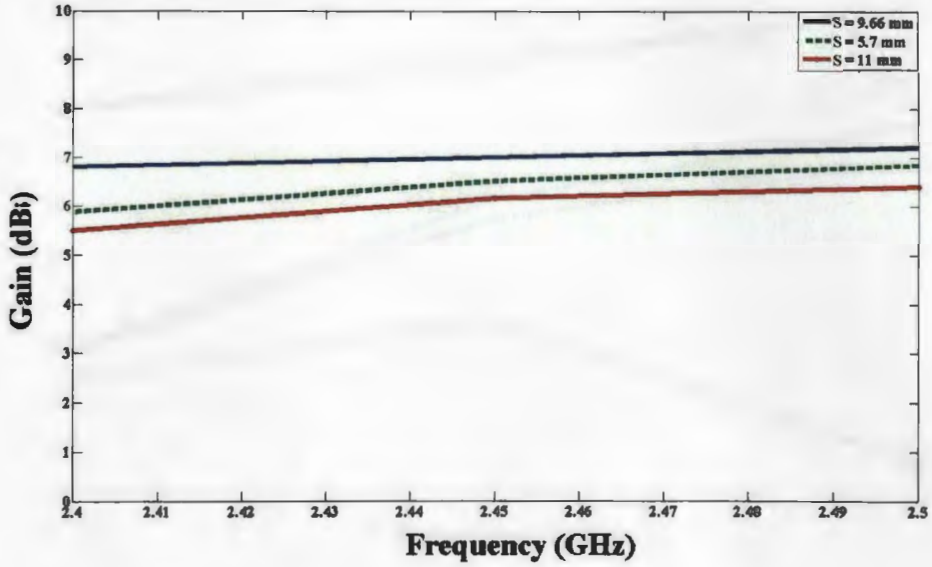


Figure 26. Simulated gain for different driver-director spacings.

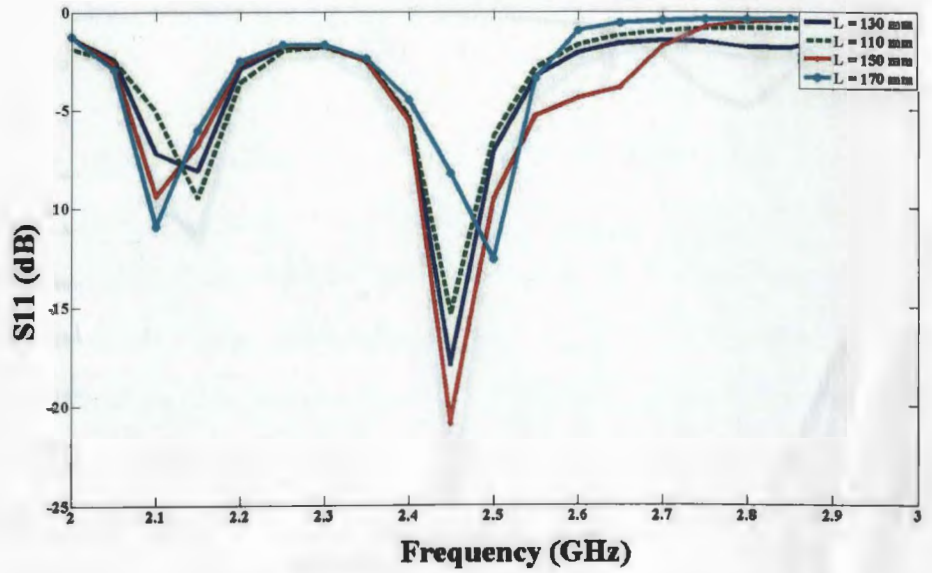


Figure 27. Simulated S-parameters for different director lengths.

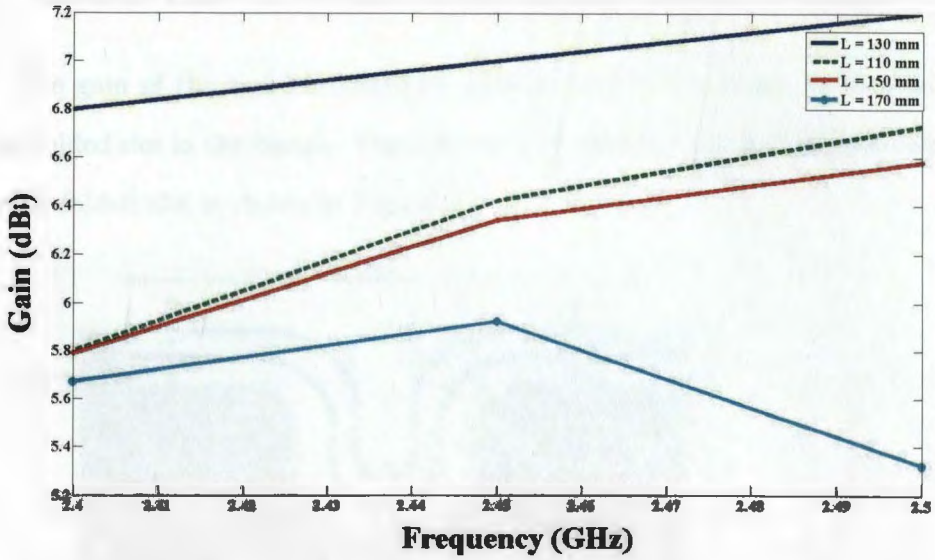


Figure 28. Simulated gain for different director lengths.

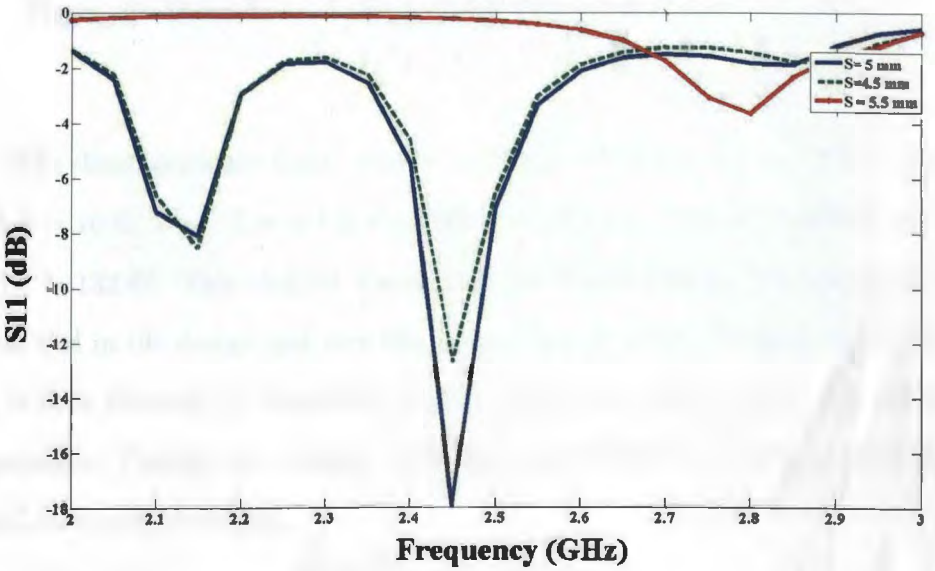


Figure 29. Simulated S-parameters for driver-ground plane spacings.

# CHAPTER 4. GAIN ENHANCEMENT DESIGN

The gain of the quasi-Landstorfer antenna can be increased by introducing a partial folded slot in the design. The schematic of the quasi-Landstorfer antenna with a partial folded slot is shown in Figure 30.

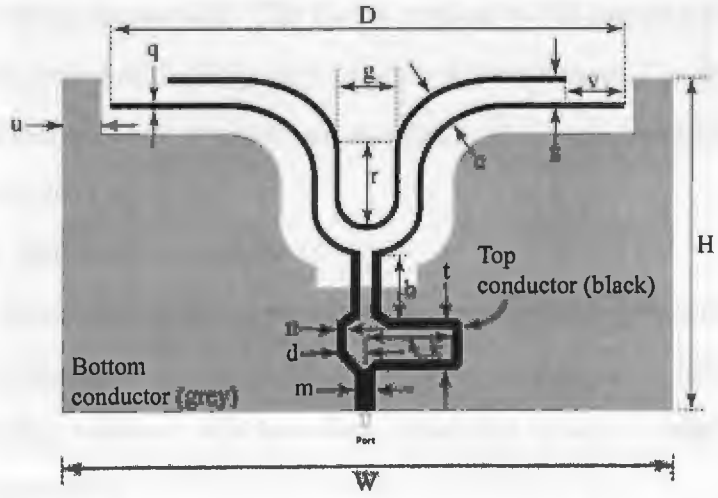


Figure 30. Quasi-Landstorfer antenna with partial slot.

The dimensions are (unit: mm):$v = 26.3, g = 9.0, q = 1.5, c = 9.5, s = 9.5, r = 20.74, b = 10.69, t = 7.2, n = 1.2, d = 3.66, k = 10.2, m = 2.4, H = 82.0, D = 114.35,$ and $W = 132.67$. This chapter starts with the theory behind the introduction of a partial slot in the design and how the partial slot increases the gain of the antenna. This is then followed by discussing the simulated $S_{11}$, radiation pattern, and gain of the antenna. Finally, the chapter concludes with a brief discussion of the proposed quasi-Landstorfer antenna.

## 4.1. Theory

In this section, the theory behind the quasi-Landstorfer antenna with a partial folded slot is presented. The discussion begins with the review of boundary conditions. Since the antenna radiates in the free space, boundary conditions are applied to find the fields in the far-field. The field is created by the currents induced in the antenna. A brief review of the Huygen's principle is also presented in this section. Then all of the aforementioned concepts are applied to the quasi-Landstorfer antenna with the partial folded slot.

### 4.1.1. Boundary conditions

Boundary conditions explain how the tangential and normal componenets of the field in one medium are related to the componenets of the field across the boundary in another medium. The boundary conditions at any interface of two mediums can be expressed as

$$\hat{n} \cdot (\bar{D}_2 - \bar{D}_1) = \rho_s \tag{10}$$

$$\hat{n} \cdot \bar{B}_2 = \hat{n} \cdot \bar{B}_1 \tag{11}$$

$$\hat{n} \times (\bar{E}_2 - \bar{E}_1) = 0 \tag{12}$$

$$\hat{n} \times (\bar{H}_2 - \bar{H}_1) = \bar{J}_s \tag{13}$$

For the fields at an interface between two lossless dielectric materials, no charge or surface current densities exist. Therefore, the normal components of $\bar{D}$ and $\bar{B}$ are continuous across the interface. Moreover, the tangential components of $\bar{E}$ and $\bar{H}$

are also continuous across the interface and the boundary conditions reduce to the following forms:

$$\hat{n} \cdot \bar{D}_1 = \hat{n} \cdot \bar{D}_2 \tag{14}$$

$$\hat{n} \cdot \bar{B}_1 = \hat{n} \cdot \bar{B}_2 \tag{15}$$

$$\hat{n} \times \bar{E}_1 = \hat{n} \times \bar{E}_2 \tag{16}$$

$$\hat{n} \times \bar{H}_1 = \hat{n} \times \bar{H}_2 \tag{17}$$

At an interface between a lossless dielectric and a perfect conductor, all the field components are zero inside the conducting region. This then leads to the following boundary condition:

$$\hat{n} \cdot \bar{D} = \rho_s \tag{18}$$

$$\hat{n} \cdot \bar{B} = 0 \tag{19}$$

$$\hat{n} \times \bar{E} = 0 \tag{20}$$

$$\hat{n} \times \hat{H} = \bar{J}_s \tag{21}$$

### 4.1.2. Huygen's principle

Let us consider electromagnetic sources be contained in a volume $V$ bounded

by surface $S$ with an outward normal $\hat{n}$ as shown in Figure 31. The fields $\bar{E}$ and $\bar{H}$ outside the region $S$ are found by removing the sources in $V$ and placing the equivalent surface current densities. This is shown in Fig. 31(b) and for discussion the magnetic current $M_s$ has been defined.

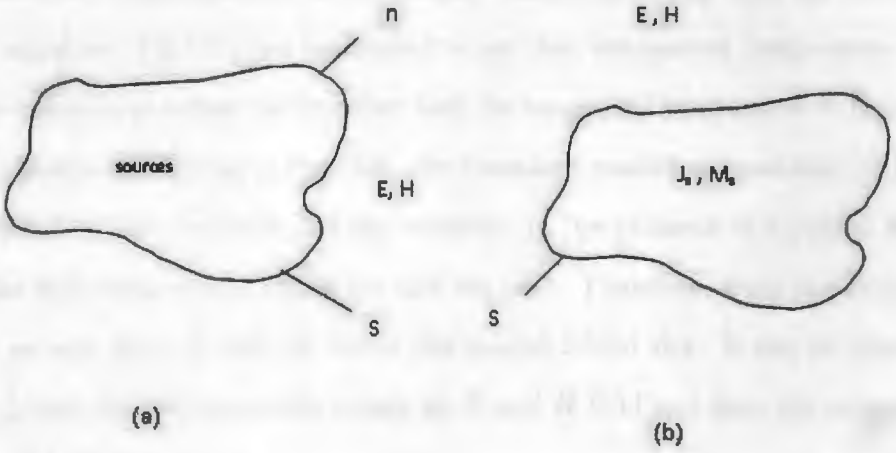


Figure 31. (a) Original problem (b) Equivalent problem using Huygen's principle.

This then leads to the following boundary condition:

$$\bar{J}_s = \hat{n} \times \bar{H}_s \tag{22}$$

$$\bar{M}_s = \hat{n} \times \bar{E}_s \tag{23}$$

In the original problem in Fig. 31(a), the fields along the surface are $\bar{E}_s$ and $\bar{H}_s$ whereas in the equivalent problem in Fig. 31(b), the fields inside the volume $V$ are zero and surface currents are given by Equations (22) and (23). By applying boundary

conditions, equations (12) and (13) give us $\hat{n} \times (\bar{H}_s - 0) = \bar{J}_s$ and $(\bar{E}_s - 0) \times \hat{n} = \bar{M}_s$ that is identical to the equations given by (22) and (23).

Let us consider $\Delta s$ to be the area of the partial folded slot of our antenna design. In Fig. 32a, the medium of the partial folded slot is air (i.e. there is no partial folded slot) whereas, in Fig. 32b, the medium of the slot is a perfect conductor (i.e. the partial folded slot is incorporated in the design). Referring to Fig. 32a, the boundary condition equation (14)-(17) can be applied to see that the normal components of $\bar{D}$ and $\bar{B}$ are continuous across the interface and the tangential component of $\bar{E}$ and $\bar{H}$ are equal. Moreover, refering to Fig. 32b, the boundary condition equations (18)-(21) can be applied to find the fields and the currents. In the presence of a partial folded slot, all the field components inside the slot are zero. Therefore, from the Huygen's principle, we can place $\bar{J}_s$ and $\bar{M}_s$ inside the partial folded slot. It can be observed that this $\bar{J}_s$ and $\bar{M}_s$ will eventually create an $\bar{E}$ and $\bar{H}$ field and thus the gain of the antenna will further increase.

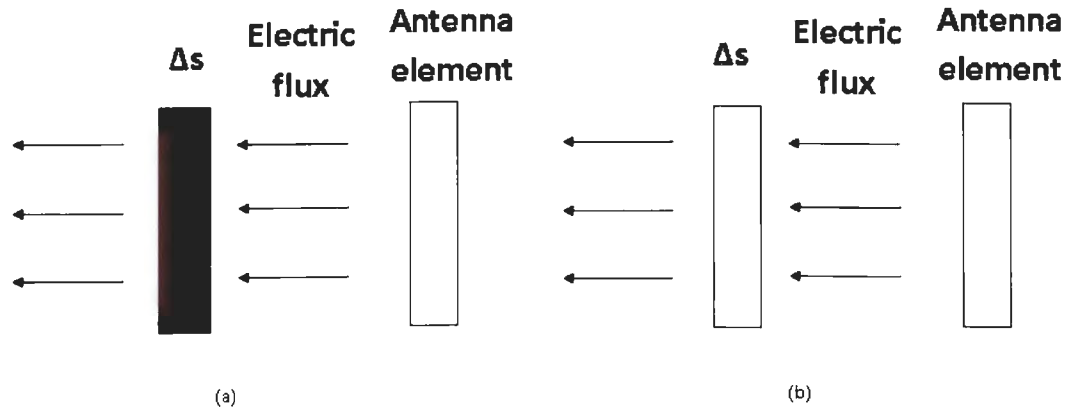


Figure 32. Partial folded slot in two different media (a) The medium of the partial folded slot of the antenna is air (b) The medium of the partial folded slot of the antenna is a perfect conductor.

### 4.2. Simulated results

The $S_{11}$ values of the quasi-Landstorfer antenna with a partial folded slot are shown in Figure 33. The antenna has a simulated return loss of -18 dB at 2.45 GHz. Therefore, the introduction of a partial folded slot does not affect the resonance of the quasi-Landstorfer antenna in Fig. 13 without a partial folded slot. The radiation pattern was simulated for the x-z and y-z planes. Figs. 34 and 35 presents the radiation pattern for the x-z and y-z planes, respectively.

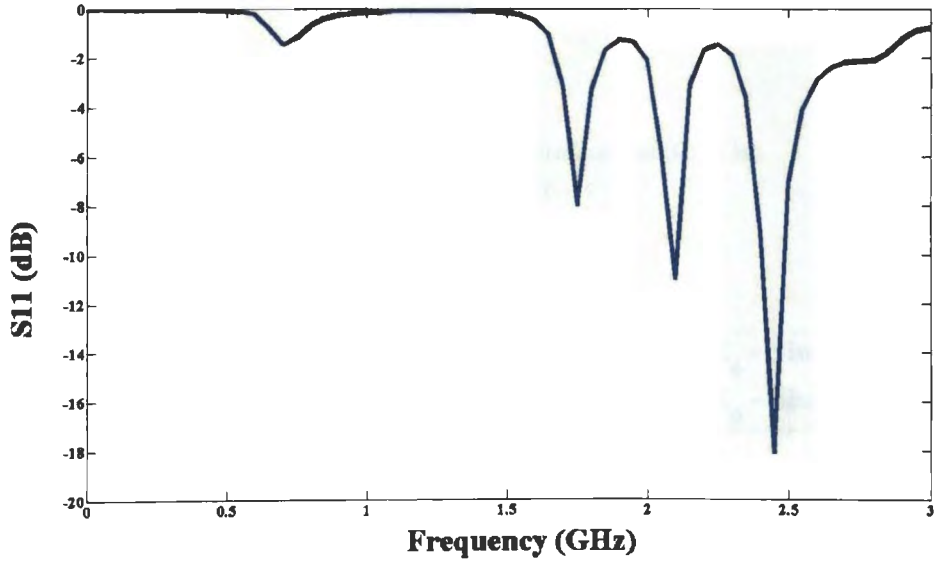


Figure 33. Simulated $S_{11}$ with partial folded slot.

The quasi-Landstorfer antenna with a partial folded slot follows the end-fire radiation pattern. Moreover, the gain of the antenna increases from 7 dBi to 8 dBi by adding the partial slots as shown in Figure 36.

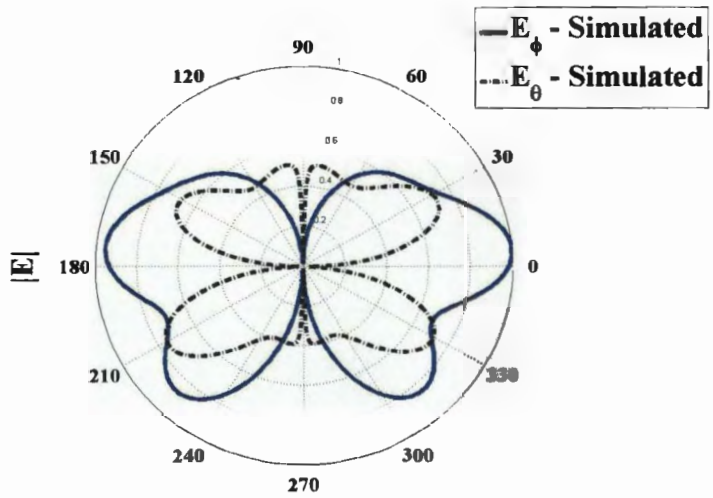


Figure 34. Simulated radiation pattern in the x-z plane at 2.45 GHz.

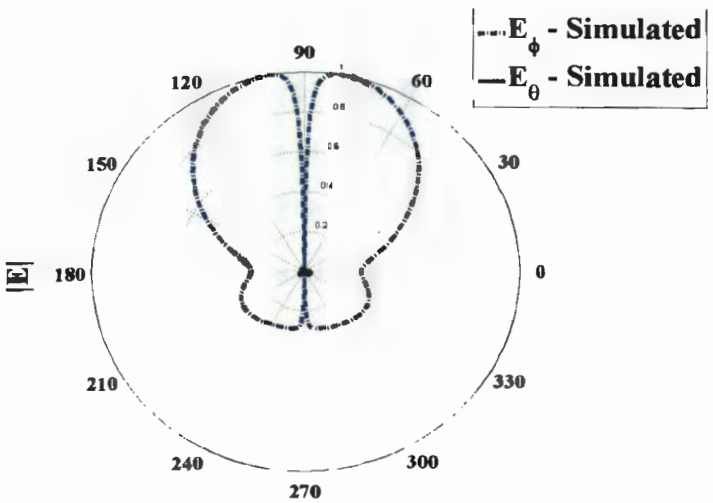


Figure 35. Simulated radiation pattern in the y-z plane at 2.45 GHz.

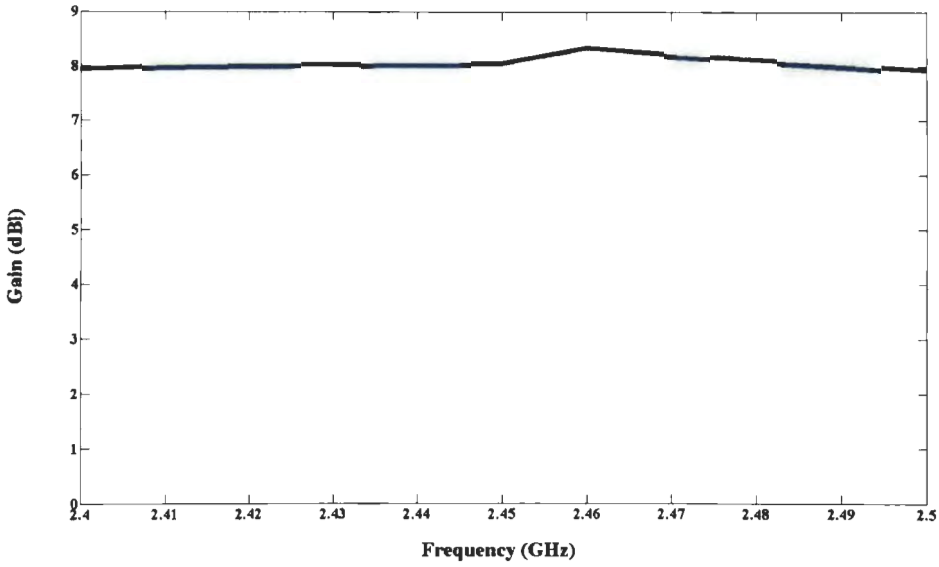


Figure 36. Simulated gain with partial folded slot.

### 4.3. Discussion

In this thesis, we presented a new printed quasi-Landstorfer antenna. The proposed antenna resembles the geometry of the quasi-Yagi antenna and the Landstorfer antenna. However, the operation of the quasi-Landstorfer antenna is different than those of the aforementioned antennas. The quasi-Yagi antenna utilizes the $TE_0$ surface-wave mode to couple the director and the driver. The $TE_0$ mode is generated by using a thick and a high dielectric constant substrate. Moreover, the $TE_0$ surface wave mode also contributes to the radiation of the quasi-Yagi antenna. The quasi-Yagi antenna has a relatively low gain and low radiation efficiency. Furthermore, the utilization of the $TE_0$ mode surface wave also restricts the quasi-Yagi antenna to be used efficiently in only the higher frequency bands and can be an inherently poor radiator at lower frequencies. The proposed quasi-Landstorfer antenna utilizes only $TEM$ modes for free-space radiation. The antenna eliminates the $TE$ surface

wave mode radiation by using a low dielectric constant substrate. Moreover, the radiation efficiency of the antenna also increases due to only the $TEM$ mode free-space radiation. The gain of the quasi-Landstorfer antenna is also higher than that of the quasi-Yagi antenna. This is because the quasi-Landstorfer antenna consists of sweeping elements whereas the quasi-Yagi antenna consists of linear dipole elements. The incorporation of the sweeping elements in the quasi-Landstorfer antenna design permits the current to travel for a longer path that eventually leads to higher gain. Therefore, the proposed quasi-Landstorfer antenna has a higher gain and higher radiation efficiency than that of the quasi-Yagi antenna. Moreover, the quasi-Landstorfer antenna is also more suitable for wireless applications at lower frequencies than the quasi-Yagi antenna.

The other antenna design that used sweeping or curved elements as the antenna elements was the Landstorfer antenna. The principle of the Landstorfer antenna is to chose the driver length to be greater than $\lambda_0$ and then shape the conductor so that the fields from the currents in the $\lambda_0$ portion add to each other whereas the fields from the currents in the additional portion cancel each other. In the proposed quasi-Landstorfer antenna, a similar concept was employed for the antenna elements. However, in the Landstorfer antenna a sweeping element was employed as the reflector to get the end-fire radiation pattern. In the quasi-Landstorfer antenna the reflector element was removed and the ground plane that was used as the reference for the microstrip input was utilized as the reflector. Therefore, the overall size of the proposed antenna is 44% smaller than that of the Landstorfer antenna. Also, in the feed network of the Landstorfer antenna, a balun with a via was used. However, the proposed quasi-Landstorfer antenna incorporates the balun in a single layer transmission line and thus eliminates the need for a via. The single-layer transmission line in the feed network simplifies the overall design of the antenna.

In this thesis, a partial folded slot is introduced in the design to enhance the gain of the antenna. To the best of the author's knowledge, the concept of adding a partial folded slot in the antenna design to increase the gain was never studied. Accordingly, the incorporation of a partial folded slot in the antenna design results in an increase of 1 dBi gain where keeping the overall size of the antenna constant. The operation of the partial folded slot in the design has been studied extensively. Furthermore, the partial folded slot can be introduced in other antennas that have an end-fire radiation pattern.

# CHAPTER 5. CONCLUSION

In this thesis, the design of a compact quasi-Landstorfer antenna has been presented. The antenna is measured to have a return loss of -43 dB at 2.45 GHz. Moreover, the size of the antenna is 44% less than that of the previous Landstorfer antennas. The antenna also exhibits a symmetric radiation pattern in the end-fire direction. The gain of the antenna was measured to be 7 dBi. Moreover, a gain enhancement design has also been presented with the overall dimensions of the antenna remaining the same. The gain enhancement design introduces a partial folded slot in the design that contributes to achieve a gain of 8 dBi. The theory of the proposed quasi-Landstorfer antenna with and without the partial folded slot has been studied extensively. The partial folded slot can also be employed in other antenna designs that have an end-fire radiation pattern. With compact size and moderate gain, the quasi-Landstorfer antenna can be widely used in WLAN applications, such as wireless communications, phased arrays, and millimeter wave applications.

In the future, particle resonators could be used in the antenna elements to reduce the overall size of the antenna. The reduction in size of the antenna will allow the antenna to be used in the array environment.

# REFERENCES


[1] C. P. Narayan, *Antennas and propagation*, Technical Publications, 2007, pp. 150-153.

[2] W. R. Deal, N. Kaneda, J. Sor, Y. Qian, and T. Itoh, "A new Quasi-Yagi antenna for planar active antenna arrays," *IEEE Transactions on Microwave Theory and Techniques*, vol. 48, no. 6, pp. 910-918, 2000.

[3] N. Kaneda, W. R. Deal , J. Sor, Y. Qian, and T. Itoh, "A broadband planar Quasi-Yagi antenna," *IEEE Transactions on Antennas and Propagation*, vol. 50, no. 8, pp. 1158-1160, 2002.

[4] F. Landstorfer, "A new type of directional antenna," *IEEE Antennas and Propagation Symposium*, Oct. 1976, pp. 169-172.

[5] A. C. K. Mak, C. R. Rowell, and R. D. Murch, "Low cost reconfigurable Landstorfer planar antenna array," *IEEE Transactions on Antennas and Propagations*, vol. 57, no. 10, pp. 3051-3061, 2009.

[6] C. A. Balanis, *Antenna Theory: Analysis and Design*, $2^{nd}$ Ed., John Wiley and Sons, Inc., Hoboken, New Jersey, 2005, pp. 577-580.

[7] W. L. Stutzman and G. A. Thiele, *Antenna Theory and Design*, $2^{nd}$ Ed., John Wiley and Sons, Inc., New York, NY, pp. 220-228.

[8] Advanced Computer Design, ADS 2009. Agilent Technologies.

[9] I. J. Bahl and P. Bhartia, *Microstrip Antennas*, $2^{nd}$ Ed., Artech House, Inc., Dedham, MA, 1982, pp. 22-27.

[10] N. G. Alexopoulos, P. B. Katehi, and D. B. Rutledge, "Substrate optimization for integrated circuit antennas," *IEEE Transactions on Microwave Theory and Techniques*, vol. MTT-31, no. 7, pp. 550-557, 1983.

[11] D. M. Pozar, "Considerations for millimeter wave printed antennas," *IEEE Transactions on Antennas and Propagation*, vol. AP-31, no. 5, pp. 740-747, 1983.

[12] Applications Computer Aided Design Program, AppCAD 2010. Agilent Technologies.

[13] T.-G. Ma, C.-W. Wang, R.-C. Hua, and J.-W. Tsai, "A modified Quasi-Yagi Antenna with a new compact microstrip-to-coplanar strip transition using artificial transmission lines," *IEEE Transactions on Antennas and Propagations*, vol. 57, no. 8, pp. 2469-2474, 2009.

[14] W. Nannan, Q. Jinghui, L. Shu, and D. Weibo, "Research on wide beamwidth and high gain Quasi-Yagi antenna," *8th International Symposium on Antennas, Propagation and EM Theory*, Kunming, China, Nov. 2008, pp. 302-305.

[15] J. M. Steyn, J. W. Odendaal, and J. Joubert, "Double dipole antenna for dual-band wireless local area networks applications," *Microwave and Optical Technology Letters*, vol. 51, no. 9, pp. 2034-2038, 2009.

[16] D. M. Pozar, *Microwave Engineering*, $2^{nd}$ Ed., John Wiley and Sons, Inc., New York, NY, August 1998, pp. 9-14.

[17] N. Kaneda, Y. Qian, and T. Itoh, "A broadband microstrip-to-waveguide transition using Quasi-Yagi antenna," *IEEE Transactions on Microwave Theory and Techniques*, vol. 47, no. 12, pp. 2562-2567, 1999.

[18] TDK RF solution Inc., www.tdkrfsolutions.com

[19] A.H. Systems Inc., www.ahsystems.com

# APPENDIX. MATLAB CODE

The following

`S_11.m`

code was used to produce the $S_{11}$ *vs. Frequency* plots that is presented in this dissertation.

The following

`Rad_pat.m`

code was used to produce the *Radiation pattern vs. Frequency* plots that is presented in this dissertation.

The following

`Gain.m`

code was used to produce the *Gain vs. Frequency* plots that is presented in this dissertation.

## `S_11.m file`

```
clc
clear all

S11_meas=[data...];
S11_sim=[data...];

figure
plot(S11_sim(:,1)./1e9,S11_sim(:,2),'-',S11_meas(:,1)./1e9,S11_meas(:,2),'.-')
xlabel('f(GHz)')
ylabel('|S_{11}| (dB)')
% axis([1.5 3.5 -25 0])
grid off
legend('Simulated','Measured')
```

## `Rad_pat.m file`

```
clc
clear all

E_phi_xz_meas=[data...];
E_theta_xz_meas=[data...];
E_phi_yz_meas=[data...];
E_theta_yz_meas=[data...];
E_phi_xz_sim=[data...];
E_theta_xz_sim=[data...];
E_phi_yz_sim=[data...];
E_theta_yz_sim=[data...];
E_phi_yz_meas_bottom=[data...];
E_theta_yz_meas_bottom=[data...];


figure
polar(E_phi_yz_sim(:,1)*pi/180,E_phi_yz_sim(:,2)./max(E_phi_yz_sim(:,2)),'-')
hold on
polar([[-90:3:90] [-90:-3:-180] [177:-3:90]]'*pi/180, [[E_phi_yz_meas];[E_phi_yz_meas_bottom]]/max(E_phi_yz_meas),'*')
polar(E_theta_yz_sim(:,1)*pi/180,E_theta_yz_sim(:,2)./max(E_phi_yz_sim(:,2)),'-')
polar([[-90:3:90] [-90:-3:-180] [177:-3:90]]'*pi/180, [[E_theta_yz_meas];[E_theta_yz_meas_bottom]]/max(E_phi_yz_meas),'.')

legend('E_{\phi} - Simulated','E_{\theta} - Simulated','E_{\phi} - Measured','E_{\theta} - Measured')
xlabel('f')
ylabel('|E|')
title('y - z plane')

figure
polar(E_theta_xz_sim(:,1)*pi/180,E_theta_xz_sim(:,2)./max(E_theta_xz_sim(:,2)),'-')
hold on
polar(E_phi_xz_sim(:,1)*pi/180,E_phi_xz_sim(:,2)./max(E_theta_xz_sim(:,2)),'-')
polar([0:3:360]'*pi/180, E_phi_xz_meas/max(E_theta_xz_meas),'.')

polar([0:3:360]'*pi/180, E_theta_xz_meas/max(E_theta_xz_meas),'*')

legend('E_{\phi} - Simulated','E_{\theta} - Simulated','E_{\phi} - Measured','E_{\theta} - Measured')
xlabel('f')
ylabel('|E|')
title('x - z plane')

% axis([-90 90 10e-5 1])
```

## Gain.m file

```
clc
clear all

f_sim=[data...];
g_sim=[data...];

f_meas=[data...];
g_meas=[data...];
```

```
xlabel('f (GHz)')
ylabel('Gain (dB)')

plot(f_sim,g_sim,f_meas,g_meas,'-')
legend('simulated','measured')
axis([2.4 2.5 0 8])
xlabel('f (GHz)')
ylabel('Gain (dB)')
title ('Gain Vs. Frequency plot')
```